COVER SHEET

NOTE: This coversheet is intended for you to list your article title and author(s) name only —this page will not appear on the Electronic Product.

Title: *Toughening of Boron Carbide Composites by Hierarchical Microstructuring*

Authors: Jingyao Dai[1]
Evan Pineda[2]
Brett Bednarcyk[2]
Jogender Singh[3]
Namiko Yamamoto[3 *]

*Corresponding author, Phone: 814-867-5775, Email: nuy12@psu.edu

Affiliations: 1. Massachusetts Institute of Technology
2. NASA Glenn Research Center
3. Pennsylvania State University

ABSTRACT

Due to a unique combination of properties including high hardness, low density, chemical and thermal stability, semi-conductivity, and high neutron absorption, boron carbide (B_4C) is a potential candidate for various applications involving extreme environment. However, B_4C's current application is limited because of its low fracture toughness. In this study, a hierarchical microstructure design with features including TiB_2 grains and graphite platelets was used to toughen B_4C by simultaneously utilizing multiple toughening mechanisms including crack deflection, bridging, and micro-crack toughening. Using field-assisted sintering technology (FAST), B_4C composites with dense and hierarchical microstructure were fabricated. Previously, the fracture toughness of fabricated B_4C composites was measured at micro-scale using micro-indentation to have up to 56% improvement. In this work, the B_4C composites' fracture toughness was characterized at macro-scale using four-point bending methods and compared with previous results obtained at micro-scale. Micromechanics modeling of fracture behaviors for B_4C-TiB_2 composites was also performed to evaluate the contributions from experimentally observed toughening mechanisms. From four-point bending tests, B_4C composites reinforced with both TiB_2 grains (~15 vol%) and graphite platelets (~8.7 vol%) exhibited the highest fracture toughness enhancement from 2.38 to 3.65 $MPa \cdot m^{1/2}$. The measured values were lower than those obtained using micro-indentation but maintained the general trends. The discrepancy between the indentation and four-point bending test results originated from the complex deformation behaviors triggered by the high contact load during indentation tests. Through micromechanics modeling, introduced thermal residual stress due to thermal expansion mismatch between B_4C and TiB_2, and weak interphases at B_4C-TiB_2 boundaries were identified as the main causes for experimentally observed toughness enhancement. These results proved the effectiveness of hierarchical microstructure designs for B_4C toughening and can provide reference for the future design of B_4C composites with optimized microstructures for further fracture toughness enhancement.

---

1. Massachusetts Institute of Technology, Cambridge, MA 02142, U.S.A.
2. NASA Glenn Research Center, Cleveland, OH 44135, U.S.A.
3. Pennsylvania State University, University Park, PA 16802, U.S.A.

INTRODUCTION

Boron carbide (B_4C) possesses a unique combination of properties including high hardness (~29.1 GPa [1]), high stiffness (Young's modulus: ~448 GPa [2]), high melting point (~2450 °C [3]), low density (2.52 g/cm^3 [1]), wear and corrosion resistance, semi-conductivity [1], and high neutron absorption capability [4], making it a suitable candidate for applications including body armor, radiation shielding, and protective coating. However, due to its intrinsically low fracture toughness (K_{IC}: ~ 2.9 MPa·m$^{1/2}$ [5]), applications of B_4C are currently limited.

Conventionally, secondary phases including various transitional metal carbides and borides such as titanium diboride (TiB_2) [6–10] and zirconium diboride (ZrB_2) [11] have been used to reinforce B_4C through toughening mechanisms like crack deflection, crack bridging, and micro-crack toughening [12]. More recently, various studies have pursued toughening of B_4C via carbon-based nanofiller reinforcement including carbon nanotubes (CNTs) [13,14] and graphene platelets (GPL) [15,16]. There have also been investigations on novel toughening mechanisms triggered by nanoporosity and nano-crystallinity [17–21], which demonstrated a fracture toughness increase up to ~75% (from 3.6 to 4.7 MPa·m$^{1/2}$) through deformation mechanisms like grain boundary sliding and nanopore compression/collapse [17].

In our study, toughening of B_4C was pursued via a hierarchical microstructure design (see Figure 1) which utilizes both secondary reinforcement phases (TiB_2) and 'soft' grain boundary phases (graphite platelets and nanocrystalline B_4C phase) [22,23]. In addition to the baseline monolithic B_4C samples, three types of B_4C composites, micro B_4C-TiB_2 composite with micron-sized TiB_2 particulate reinforcement, micro/nano B_4C with sub-micron graphite platelets, and micro/nano B_4C-TiB_2 both sub-micron TiB_2 and graphite platelet reinforcements respectively, were fabricated. The hardness and fracture toughness of these composites were measured using micro-indentation. Compared with the baseline B_4C sample (K_{Ic}: 2.98 MPa·m$^{1/2}$), the fabricated micro/nano B_4C, micro B_4C-TiB_2, and micro/nano B_4C-TiB_2 samples exhibited enhanced fracture toughness of up to 4.16, 4.67, and 4.65 MPa·m$^{1/2}$ respectively due to toughening mechanisms including graphite delamination, crack deflection/bridging. While the micro/nano B_4C and micro B_4C-TiB_2 samples showed hardness degradation from 32.46 GPa to 18.19 and 29.43 GPa, the micro/nano B_4C-TiB_2 samples maintained high hardness (31.88 GPa) while demonstrating toughness enhancement.

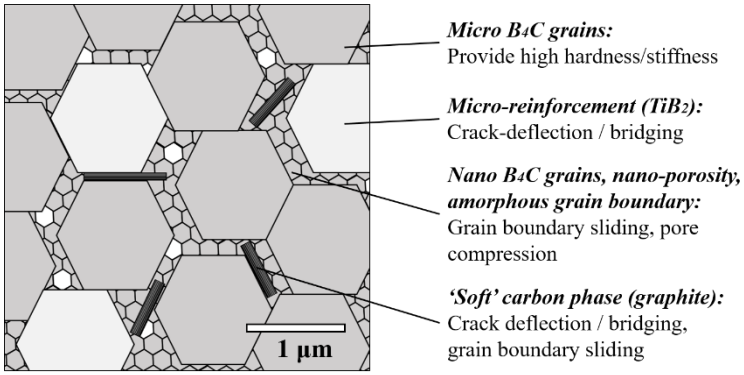

Figure 1. Schematics of hierarchical microstructures of B_4C composites [23].

Here, we will address two main challenges that remained: 1) the fracture toughness enhancement was measured at micro-scale using indentation methods and may not translate to macro-scale toughening behaviors, 2) multiple toughening mechanisms coexist for the fabricated B_4C composites with hierarchical microstructures, making it difficult to identify the toughening effects of individual toughening mechanisms. First, macro-scale standardized fracture toughness measurement via four-point bending tests was carried out for macro-scale microstructure-property relations of hierarchical micro-structured B_4C composites. Second, micromechanics modeling of fracture behaviors was performed on B_4C composites reinforced with TiB_2 reinforcements using a micromechanics analysis code MAC/GMC with an embedded crack-band model. Effects of weak B4C-TiB2 interfaces and thermal residual stresses created by the large coefficient of thermal expansion (CTE) mismatch were investigated.

MATERIALS AND METHODS

Macro-scale Fracture Toughness Characterization

Field-assisted sintering technology (FAST) was used to fabricate B_4C composite samples for macro-scale standardized fracture toughness characterization. For baseline monolithic B_4C samples, commercially available B_4C micro-powders (H.C. Stark, Grade HS, particle size: ~0.6-1.2 μm) were sintered at 2100 °C with 100 °C/min heating rate and 45 MPa applied pressure for 20 minutes. For micro/nano B_4C samples, 10 and 20 vol% of B_4C-C nano-powders (US-Nano Inc, 55 wt% B_4C and 45 wt% graphitic carbon, particle size: ~45-55 nm) were used to introduce graphite platelets between B_4C grains and sintered under the same condition as the baseline B_4C samples. For micro and micro/nano B_4C-TiB_2 composites, the introduction of TiB_2 reinforcement was achieved using an in-situ reaction approach according to reaction (1).

$$B_4C + 2\ TiO_2 + 3\ C \rightarrow 2\ TiB_2 + 4\ CO \qquad (1)$$

Three micro B_4C-TiB_2 composites with 5, 10, and 15 vol% TiB_2 reinforcements were sintered using B_4C micro-powders, TiO_2 nano-powders (US-Nano Inc, particle size: ~40 nm, anatase phase), and carbon black nano-powders (Alfa Aesar, particle size: ~42 nm). For micro/nano B_4C-TiB_2 composites, B_4C-C nano-powders were used to provide the carbon source for reaction (1) instead of the carbon black powders to form sub-micron sized TiB_2 grains of 5, 10, and 15 vol% as well as introducing graphite platelets between B_4C grains. For all the fabricated samples, the starting powders were mixed in methanol using a planetary ball-mill (Tencan XQM-0.4A) at 600 rpm for one hour before drying in air at 110 °C for 12 hours. FAST sintering was performed using a 25-ton loading capacity FAST unit (FCT HP D25).

In our previous works [22,23], the fabricated micro and micro/nano B_4C-TiB_2 composites exhibited micro-structure inhomogeneity after the reactive sintering process. The cause of such behavior was identified previously by Huang et al to be incomplete partial reaction due to early application of pressure [9,10]. The intermediate products, boron trioxide (B_2O_3) and carbon, formed according to reaction (2) at ~1600 °C require a higher ~2000 °C temperature to form B_4C according to reaction (3)

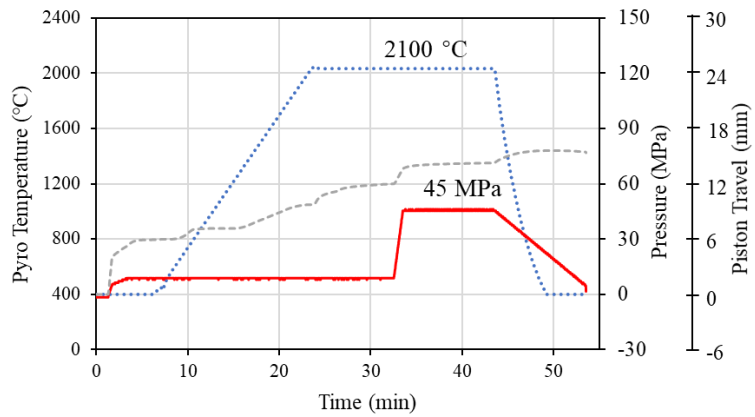

Figure 2. Representative sintering profile with a degassing step.

via carbothermal reduction [24–26]. The applied pressure resulted in higher reaction rate and better densification behaviors near the edges of the samples, inhibiting complete reaction at the center, thus causing the observed inhomogeneity.

$$2.5\ B_4C + 3\ TiO_2 \rightarrow 3\ TiB_2 + 2\ B_2O_3 + 2.5\ C \tag{2}$$

$$2\ B_2O_3 + 7\ C \rightarrow B_4C + 6\ CO \tag{3}$$

To enable fabrication of samples with homogeneous microstructures for macro-scale fracture toughness testing, a modified sintering profile with a 9-minute degassing step (see Figure 2) was used for reactive sintered micro and micro/nano B_4C-TiB_2 composites. With the updated sintering profile, samples with near full density and homogenous microstructures were successfully fabricated. Detailed density values of sintered samples can be found in our previous works [23,27].

Macro-scale fracture toughness measurement was carried out using the surface crack four-point bending method according to ASTM standard C-1412 [28]. Using a

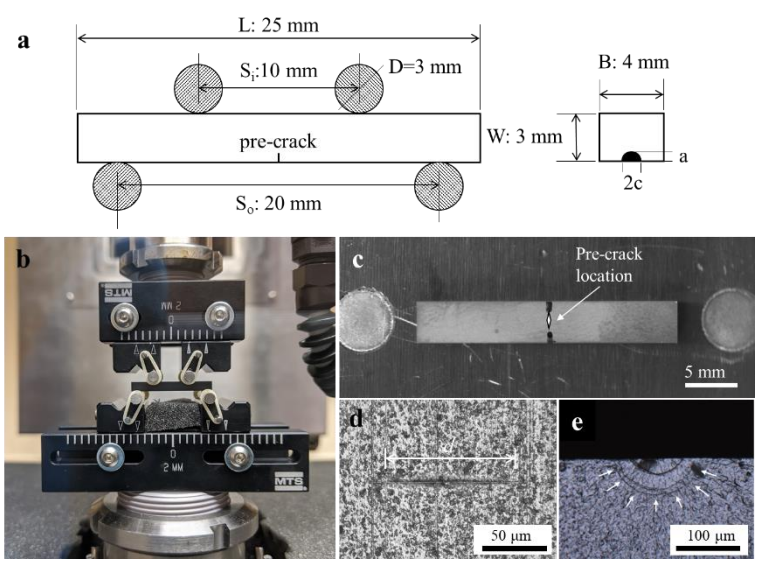

Figure 3. (a) Schematics of test fixture, specimen, and pre-crack location. (b) four-point bending test set-up, (c) image of a beam sample and pre-crack location, (d) a typical Knoop indentation impression on sample surface, (e) typical pre-crack geometry observed after bending tests

Knoop indenter tip, a surface pre-crack was created with a 2 kgf load on the surface with 4 mm width on each machined beam specimen (25 mm × 4 mm× 3 mm), perpendicular to specimens' long axis (see Figure 3). After pre-cracking, the indented surface was polished to remove the indentation impression and residual stress layer near the surface. The four-point bending tests were conducted after drying the specimens at 110 °C for at least one hour in air using an MTS Criterion electro-mechanical universal tester. Using a bending fixture with 20 mm and 10 mm outer and inner roller spans, the samples were loaded through a constant 0.02 mm/s crosshead speed equivalent to ~70-80 N/s loading rate. At least five beam specimens were tested for each type of sample. After fracture, the pre-crack geometry for each beam specimen was examined using optical microscopy and used to calculate fracture toughness according to equation (4).

$$K_{Isc} = Y\left[\frac{3\,P_{max}(S_o - S_i)10^{-6}}{2\,BW^2}\right]\sqrt{a} \tag{4}$$

Where K_{Isc} is the fracture toughness measured using the surface crack method, Y is the stress intensity factor calculated from the pre-crack geometries, P_{max} is the maximum force (fracture load), S_o and S_i are the outer and inner spans of the bending fixture, B and W are the width and thickness of the beam specimens, and a is the depth of the pre-crack.

Micromechanics Modeling of Fracture Behaviors

Micromechanics modeling of fracture behaviors was conducted for B_4C composites reinforced with TiB_2 (micro and micro/nano B_4C-TiB_2 composites) using the high-fidelity generalized method of cells (HFGMC) [29–31] incorporated in the micromechanics analysis code (MAC/GMC) developed by NASA Glenn Research Center [32,33]. To model the progressive failure of B_4C-TiB_2 composites, crack band model, which was initially developed to model failure of concrete [34] and later used for polymer and ceramic failure modeling [35–37], was used in this study.

2-D representative volume elements (RVEs) constructed from SEM images of fabricated micro and micro/nano B_4C-TiB_2 were used for the fracture modeling. The original SEM images of B_4C-TiB_2 composites were first converted into two-phase RVEs using ImageJ's binary function. As B_4C exhibited mostly trans-granular fracture due to its strong grain boundaries [23], the two-phase RVEs which ignored the polycrystalline morphology are sufficient for the failure modeling in this study. Using an in-house Matlab code, weak interphases were introduced at B_4C-TiB_2 interfaces

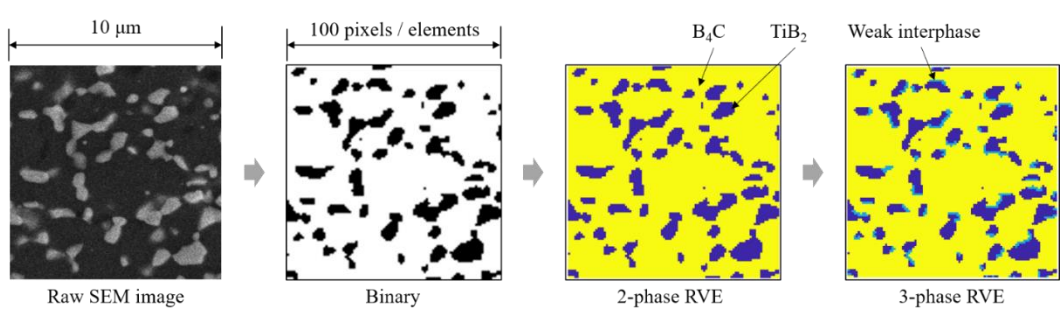

Figure 4. Representative process for the construction of RVEs from SEM images for a micro/nano B_4C-TiB_2 composite with ~15 vol% TiB_2 introduction

Table 1. Mechanical and thermal properties of B_4C and TiB_2 used for MAC/GMC modeling

	E (GPa)	ν	α (K^{-1})	ε_{fail}	σ_{fail} (GPa)	K_{Ic} ($MPa \cdot m^{1/2}$)	G_I (J/m^2)	Sub-cell size H (μm)
B_4C [1,2]	432.6	0.151	5.7×10^{-6}	0.5	2.16	2.9	19	0.1
TiB_2 [38]	584.7	0.106	8.7×10^{-6}	0.4	2.34	5.7	54.9	0.1
Interphase	432.6	0.151	5.7×10^{-6}	0.3	1.30	1.7	6.8	0.1

covering ~25% of the B_4C-TiB_2 interfaces to form three-phase RVEs (see Figure 4) to study the effects of the "soft" carbon phases on the failure behaviors of B_4C-TiB_2 composites.

To simplify the model, all three phases (B_4C, TiB_2, and weak interphase) modeled were treated as linear elastic, isotropic materials before failure. For B_4C and TiB_2, the elastic modulus, Poisson's ratio, coefficient of thermal expansion (CTE), and fracture toughness from previous literature were used (see Table 1). To model the failure behavior of B_4C and TiB_2, only mode-I fracture under tensile loading with linear softening traction-separation behaviors were used. The input parameters for the crack-band model, the slope of the softening traction-separation curves, were calculated using the selected failure strength and the mode-I critical energy release rate calculated from the materials' fracture toughness. As micro-scale strength values of B_4C and TiB_2 are not readily available, a parametric trial study was used to determine the 0.5% and 0.4% failure strain used for B_4C and TiB_2 respectively, a combination that resulted in trans-granular fracture in the modeled RVEs resembling the observed fracture behaviors. For the weak interphases, the same elastic, thermal, and post-failure softening slope were used, with failure strain/strength reduced to 60% of the strength of B_4C matrix.

The RVEs were subjected to uniaxial tensile strain up to 0.5% under plane strain condition to model the mechanical responses of the B_4C-TiB_2 composites. The residual stress created by the large CTE mismatch between B_4C matrix and TiB_2 reinforcements was modeled through a cooling load from 1000 to 23 °C without application of external loading before the uniaxial tension. Since constant CTE values were used for B_4C, TiB_2 and the weak interphases, the starting temperature of the cooling section was selected to create similar levels of tensile residual stress (~1.5 GPa) observed in past studies at B_4C-TiB_2 interfaces [6]. To study the effects of weak interphases and thermal residual stress, three cases were modeled for the micro B_4C-TiB_2 composite RVEs with ~15 vol% TiB_2: 1) without cooling, without weak interphases, 2) with cooling, without weak interphases, and 3) with cooling, with weak interphases. The effect of individual deformation mechanisms was studied by comparing the stress-strain relations, stress/strain fields obtained from the modeling.

RESULTS

Macro-scale Fracture Toughness Measurement

Using updated sintering profiles with the degassing step, B_4C composites with homogeneous microstructure and near full density (> 97% relative density) have been successfully fabricated. More details on the density values, grain size, and microstructure of the sintered B_4C composites can be found in our previous work [22,23,27]. The fracture toughness results obtained from four-point bending tests for

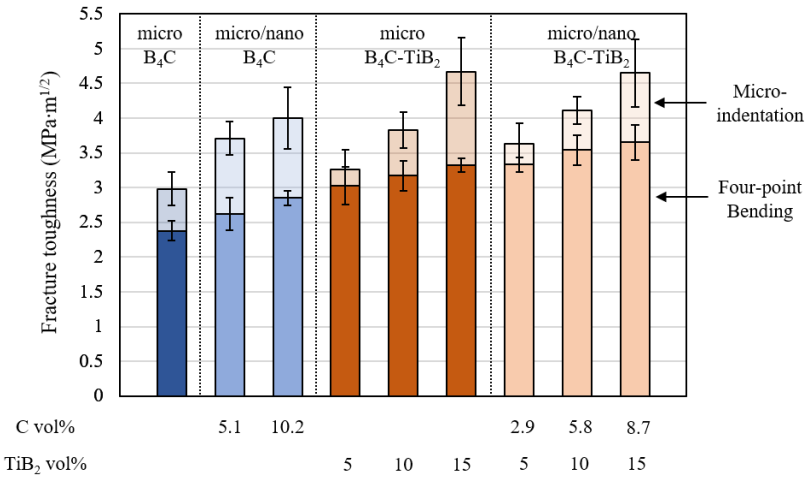

Figure 5. Fracture toughness measured using micro-indentation and four-point bending methods for fabricated B_4C composites [27]

fabricated B_4C samples were summarized and compared with fracture toughness previously measured using micro-indentation method in Figure 5.

For micro B_4C samples with densely packed grains of ~3 µm ferret diameter, the average fracture toughness measured by four-point bending was 2.38 MPa·m$^{1/2}$ (2.98 MPa·m$^{1/2}$ by micro-indentation). With 10 and 20 vol% addition of B_4C-C nano-powders, the micro/nano B_4C samples demonstrated enhanced fracture toughness of 2.62 and 2.85 MPa·m$^{1/2}$ respectively. The increase can be attributed to the increasing volume fractions of graphite formed from the nano-sized graphitic carbon in the B_4C-C nano-powders which triggered toughening mechanisms including crack deflection and graphite delamination. Higher toughness enhancement was achieved for micro and micro/nano B_4C-TiB_2 composites with fracture toughness values up to 3.32 and 3.65 MPa·m$^{1/2}$ for micro and micro/nano B_4C-TiB_2 composites with 15 vol% TiB_2 respectively. Such improvement resulted from crack deflection by the tougher TiB_2

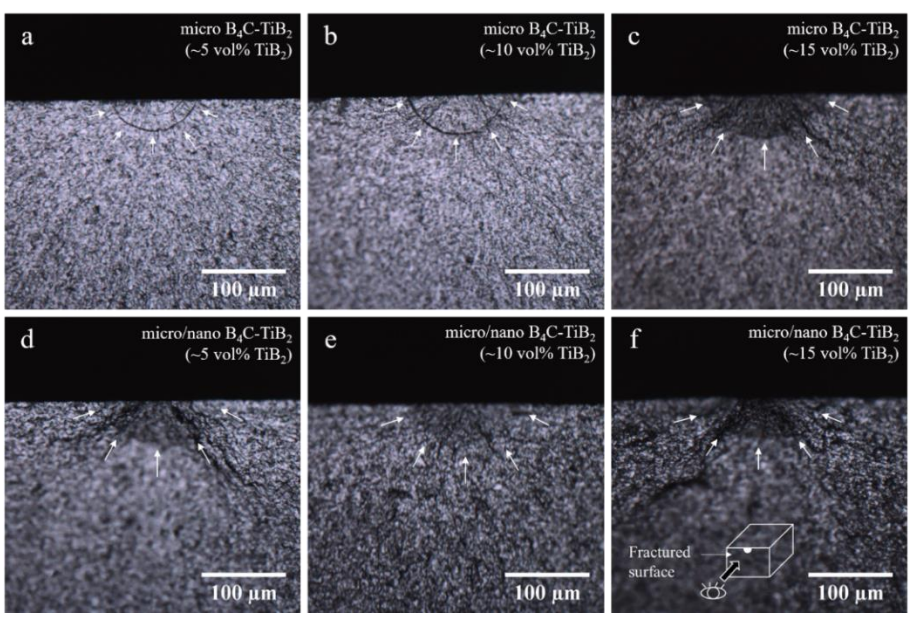

Figure 6. Images of fractured surfaces at pre-crack location of (a-c) micro B_4C-TiB_2 with ~5, 10, 15 vol% TiB_2, (d-f) micro/nano B_4C-TiB_2 with ~5, 10, 15 vol% TiB_2

phases as well as the micro-crack toughening triggered by the large CTE mismatch between B_4C matrix and TiB_2 reinforcements, both mechanisms previously confirmed using SEM and TEM inspection on indented samples [23]. The enhanced crack deflection behavior by higher volume fraction of TiB_2 was also further confirmed by the rougher fractured surfaces observed on B_4C-TiB_2 composites tested using four-point bending with higher TiB_2 volume fractions (see Figure 6). The higher fracture toughness measured for micro/nano B_4C-TiB_2 composites compared to its micro B_4C-TiB_2 composite counterparts potentially resulted from the additional toughening effect of formed graphite platelets.

Comparing the fracture toughness values measured using the micro-indentation and the macro-scale four-point bending tests, the overestimation of fracture toughness was observed consistently for all sample types. Such behavior may be caused by the additional deformation behaviors triggered by the high compressive load (in the range of ~30 GPa) beneath the indentation impressions including shear band formation in B_4C grains and in-elastic deformation/dislocations inside TiB_2 grains which provided more energy absorption mechanisms that are absent during four-point bending tests (with ~ 400 MPa tensile load near pre-crack locations).

Effects of Thermal Residual Stress and Weak Interphases on Fracture Behaviors

Previous modeling studies on fracture behaviors of B_4C-TiB_2 composites suggested two main contributing factors for the observed fracture toughness enhancement: weak interphases and thermal residual stress [6,38,39]. By modeling the fracture behaviors of micro B_4C-TiB_2 composites with 15 vol% TiB_2 under three conditions, 1) without cooling, with weak interphases, 2) with cooling, without weak interphases, and 3) with cooling, with weak interphases, the effects of weak interphases and residual stress were analyzed.

First, without thermal cooling and introduction of weak interphases, the micro B_4C-TiB_2 composite RVEs (15 vol% TiB_2) behaved in a mostly linear elastic manner before

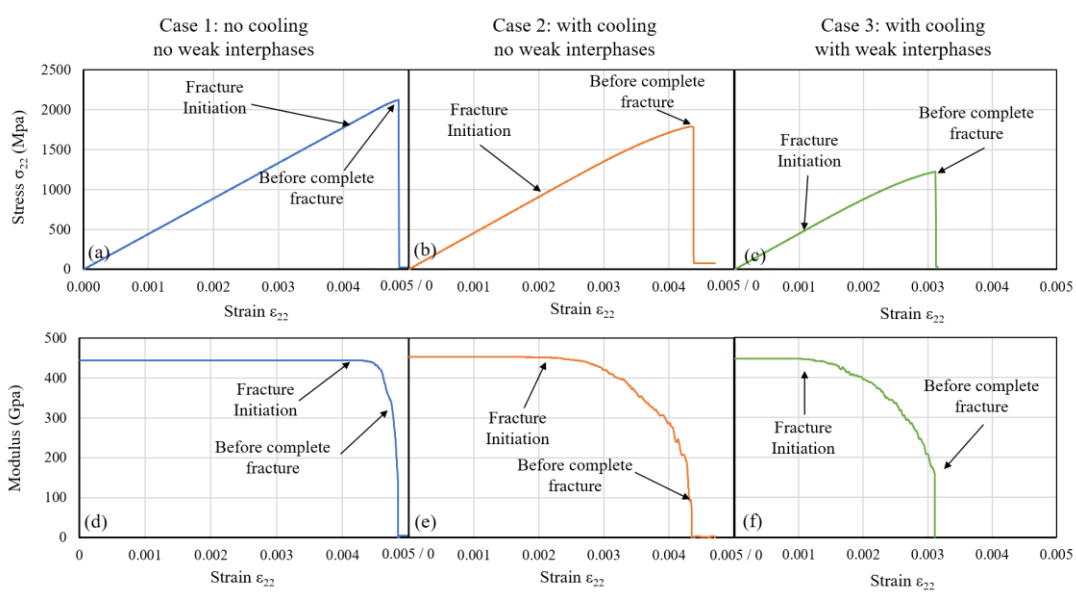

Figure 7. Representative stress-strain and modulus-strain results of a B_4C-TiB_2 composite (~15 vol% TiB_2) RVEs (a, d) with no cooling and no weak interphases, (b, e) with cooling but no weak interphases, and (c, f) with both cooling and weak interphases.

onset of fracture at ~0.41% tensile strain (~1800 MPa tensile stress, see Figure 7 (a, d)). High stress level originated from the stiffness contrast between B_4C and TiB_2 and the irregular shapes of TiB_2 grains can be seen inside and near TiB_2 particles right before fracture initiation (see Figure 8 (a)). Further loading led to limited progressive failure behavior in the form of micro-crack formation at B_4C-TiB_2 interfaces (see Figure 8 (d)) before coalescence of the micro-cracks that led to complete fracture of the RVEs. Without thermal residual stress and weak interphases, the modeled micro-cracking behavior was limited and could be solely attributed to the stress concentration around TiB_2 grains due to grain geometry and stiffness/strength contrast.

Second, when cooling load was applied, the micro B_4C-TiB_2 composite RVEs (without weak interphases) exhibited enhanced non-linear stress-strain behaviors (see Figure 7 (b, e)). Fracture initiation happened at a lower tensile strain of ~0.21%. While the RVEs for the case without thermal load only sustained limited in-elastic deformation before complete fracture, with the applied cooling load, the RVEs sustained ~0.2% increase in tensile strain before complete failure at ~0.4% tensile strain. From the stress/strain field results (Figure 8 (b, e)), high residual stress can be identified with tensile stress up to ~2.0-2.4 GPa inside and near TiB_2 grains and compressive stress of ~500 MPa in B4C matrix surrounding the TiB_2 grains. The high contrast in stress state triggered early onset of fracture and the contained micro-crack growth followed, contributing to the enhanced progressive failure behavior.

Third, when both thermal residual stress and weak interphases were introduced, micro-cracking initiated at a low tensile strain of ~0.1% (see Figure 7 (c, f)) due to the low failure strain of the introduced weak interphases. When further loaded, the RVEs experienced progressive failure through micro-crack growth at tensile strain between 0.1% and 0.3%. Like the case with cooling load but without weak interphases, the micro-crack coalescence was delayed by the compressive stress in the B_4C matrix surrounding the TiB_2 grains (see Figure 8 (c, f)). However, compared to the case without weak interphases, the RVEs with weak interphases demonstrated much higher local

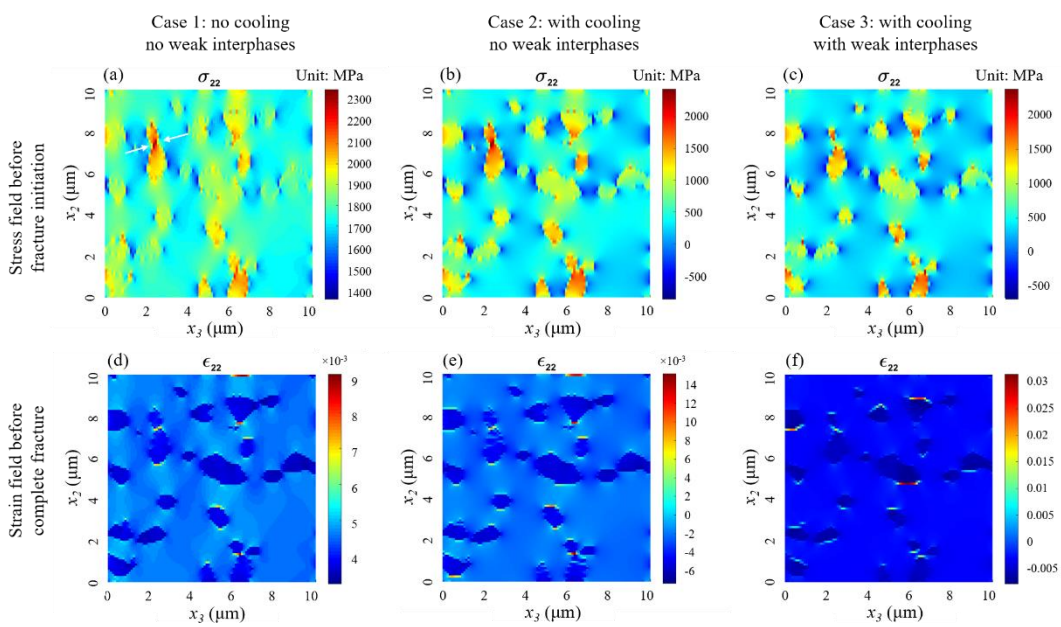

Figure 8. Representative stress (before fracture iniation) and strain (before complete fracture) field results of a B_4C-TiB_2 composite (~15 vol% TiB_2) RVEs RVEs (a, d) with no cooling and no weak interphases, (b, e) with cooling but no weak interphases, and (c, f) with both cooling and weak interphases.

strain in the tensile direction within the weak interphases (up to ~3.0%, see Figure 8 (f)) despite the lower global tensile strain.

While the micro-cracking and transgranular fracture behaviors observed in fabricated B_4C-TiB_2 composites were captured in all three cases modeled in this study, the extensive progressive failure behaviors were only achieved with the introduction of thermal residual stress. The high tensile residual stress of ~1.5 GPa inside TiB_2 grains and at B_4C-TiB_2 interfaces promoted micro-cracking, while the compressive residual stress of ~500 MPa within the surrounding B_4C matrix delayed the coalescence of micro-cracks. Such progressive failure behavior was further enhanced by the existence of weak interphases along B_4C-TiB_2 boundaries which allowed micro-crack initiation at lower load. These modeled behaviors aggreed with experimental observations and offered insights for further fracture toughness improvement for B_4C-TiB_2 composites.

CONCLUSION AND FUTURE WORK

In this study, hierarchically micro-structured B_4C composites with homogeneous microstructures were fabricated and tested for fracture toughness using macro-scale standardized four-point bending method. For micro/nano B_4C samples with graphite platelet formation, micro B_4C-TiB_2 composites with micron-sized TiB_2 grains, and micro/nano B_4C-TiB_2 composites with both sub-micron sized TiB_2 grains and graphite platelets, fracture toughness enhancement from 2.38 $MPa{\cdot}m^{1/2}$ to 2.85, 3.32, and 3.65 $MPa{\cdot}m^{1/2}$ were observed respectively. These results obtained from macro-scale testing, while exhibiting the same trends, were lower than the values previously measured using micro-indentation method. We attributed such discrepancy to the mixed-mode fracture behaviors and comples deformation mechanisms triggered by the high compressive load during the indentation tests. Using micromechanics modeling, the effects of thermal residual stress and weak interphases on fracture behaviors of B_4C-TiB_2 composites were investigated. The residual stress originated from the high CTE mismatch between B_4C and TiB_2 was found to contribute to enhanced and sustained micro-cracking behavior. Such behavior was further improved when weak interphases were present which led to early onset of micro-cracking, thus more extensive progressive failure behaviors. These results, combined with our previous works on hierarchically microstructured B_4C composites [22,23], can provide useful reference for the future design of strong and tough B_4C composites.

For future work, other material properties including impact resistance, thermal, and electrical properties for the hierarchically micro-structured B_4C composites can be measured to establish more in-depth microstructure-property relations. Micromechanics modeling of fracture behaviors can also be conducted on RVEs with polycrystalline microstructures to include the effects of grain boundaries and anisotropic properties of individual grains. Based on existing experimental and simulation data, the proposed microstructure designs for hierarchically micro-structure B_4C composites can also be further optimized to realize fracture toughness enhancement while preserving materials' high hardness and strength.

AKNOWLEDGEMENT

This material is based upon research partly supported by the U. S. Office of Naval Research under award number N000141712361. The authors are thankful for technical support from Charis Lin, Ricardo Braga Nogueira Branco, and Austin (Kirk) Heller from the Department of Aerospace Engineering (PSU), Kevin Busko and Petr Kolonin from the Applied Research Lab (PSU), Julie Anderson, Ke Wang, Haiying Wang, Jenny Gray, Manuel Villalpando, Tim Tighe, Beth Last, Trevor Clark, and Nichole Wonderling from Materials Characterization Lab (PSU).

REFERENCES

1. Thévenot, F. "Boron Carbide-A Comprehensive Review." *Journal of the European Ceramic Society*, Vol. 6, No. 4, 1990, pp. 205–225.
2. Murthy, S. R. "Elastic Properties of Boron Carbide." *Journal of Materials Science Letters*, Vol. 4, No. 5, 1985, pp. 603–605.
3. Bauccio, M. *ASM Engineered Materials Reference Book*. ASM International, 1994.
4. *Boron and Refractory Borides*. Springer Berlin Heidelberg, 1977.
5. Hyukjae Lee, R. F. S. "Hardness and Fracture Toughness of Pressureless-Sintered Boron Carbide (B4C)." *Journal American Ceramic Society*, Vol. 85, No. 5, 2002, pp. 1291–1293.
6. Sigl, L. S., and Kleebe, H. -J. "Microcracking in B 4 C-TiB 2 Composites." *Journal of the American Ceramic Society*, Vol. 78, No. 9, 1995, pp. 2374–2380.
7. Skorokhod, V., and Krstic, V. D. "High Strength-High Toughness B4C-TiB2 Composites." *Journal of Materials Science Letters*, Vol. 19, No. 3, 2000, pp. 237–239.
8. Yamada, S., Hirao, K., Yamauchi, Y., and Kanzaki, S. "High Strength B4C- TiB2 Composites Fabricated by Reaction Hot-Pressing." *Journal of the European Ceramic Society*, Vol. 23, No. 7, 2003, pp. 1123–1130.
9. Huang, S. G., Vanmeensel, K., Malek, O. J. A., Van der Biest, O., and Vleugels, J. "Microstructure and Mechanical Properties of Pulsed Electric Current Sintered B4C-TiB2 Composites." *Materials Science and Engineering A*, Vol. 528, No. 3, 2011, pp. 1302–1309.
10. Huang, S. G., Vanmeensel, K., Van der Biest, O., and Vleugels, J. "In Situ Synthesis and Densification of Submicrometer-Grained B4C-TiB2 Composites by Pulsed Electric Current Sintering." *Journal of the European Ceramic Society*, Vol. 31, No. 4, 2011, pp. 637–644.
11. Baharvandi, H. R., Hadian, A. M., Abdizadeh, A., and Ehsani, N. Investigation on Addition of ZrO2-3 Mol% Y2O 3 Powder on Sintering Behavior and Mechanical Properties of B 4C. No. 41, 2006, pp. 5269–5272.
12. Suri, A. K., Subramanian, C., Sonber, J. K., and Ch Murthy, T. S. R. Synthesis and Consolidation of Boron Carbide: A Review. *International Materials Reviews*. 1. Volume 55, 4–38.
13. Kobayashi, T., Yoshida, K., and Yano, T. "Microstructure, Mechanical and Thermal Properties of B4C/CNT Composites with Al Additive." *Journal of Nuclear Materials*, Vol. 440, Nos. 1–3, 2013, pp. 524–529.
14. Yavas, B., Sahin, F., Yucel, O., and Goller, G. "Effect of Particle Size, Heating Rate and CNT Addition on Densification, Microstructure and Mechanical Properties of B4C Ceramics." *Ceramics International*, Vol. 41, No. 7, 2015, pp. 8936–8944.
15. Tan, Y., Zhang, H., and Peng, S. "Electrically Conductive Graphene Nanoplatelet/Boron Carbide Composites with High Hardness and Toughness." *Scripta Materialia*, Vol. 114, 2016, pp. 98–102.
16. Liu, L., Wang, Y., Li, X., Xu, L., Cao, X., Wang, Y., Wang, Z., Meng, C., Zhu, W., and Ouyang, X. "Enhancing Toughness in Boron Carbide with Reduced Graphene Oxide." *Journal*

of the American Ceramic Society, Vol. 99, No. 1, 2016, pp. 257–264.
17. Madhav Reddy, K., Guo, J. J., Shinoda, Y., Fujita, T., Hirata, A., Singh, J. P., McCauley, J. W., and Chen, M. W. "Enhanced Mechanical Properties of Nanocrystalline Boron Carbide by Nanoporosity and Interface Phases." *Nature Communications*, Vol. 3, 2012, p. 1052.
18. Guo, D., Song, S., Luo, R., Goddard, W. A., Chen, M., Reddy, K. M., and An, Q. "Grain Boundary Sliding and Amorphization Are Responsible for the Reverse Hall-Petch Relation in Superhard Nanocrystalline Boron Carbide." *Physical Review Letters*, Vol. 121, No. 14, 2018.
19. Xia, Z., Riester, L., Curtin, W. A., Li, H., Sheldon, B. W., Liang, J., Chang, B., and Xu, J. M. "Direct Observation of Toughening Mechanisms in Carbon Nanotube Ceramic Matrix Composites." *Acta Materialia*, Vol. 52, No. 4, 2004, pp. 931–944.
20. Xia, Z., Riester, L., Sheldon, B. W., Curtin, W. a, Liang, J., Yin, a, and Xu, J. M. "Mechanical Properties of Highly Ordered Nanoporous Anodic Alumina Membranes." *Analysis*, Vol. 6, No. 2, 2004, pp. 131–139.
21. Dai, J., Singh, J., and Yamamoto, N. "Nonbrittle Nanopore Deformation of Anodic Aluminum Oxide Membranes." *Journal of the American Ceramic Society*, Vol. 101, No. 5, 2018, pp. 2170–2180.
22. Dai, J., Singh, J., and Yamamoto, N. Toughening of Boron Carbide Composites with Hierarchical Microstructuring. No. 1 PartF, 2020.
23. Dai, J., Singh, J., and Yamamoto, N. "Fabrication and Characterization of FAST Sintered Micro/Nano Boron Carbide Composites with Enhanced Fracture Toughness." *Journal of the European Ceramic Society*, 2020.
24. Alizadeh, A., Taheri-Nassaj, E., and Ehsani, N. "Synthesis of Boron Carbide Powder by a Carbothermic Reduction Method." *Journal of the European Ceramic Society*, Vol. 24, Nos. 10–11, 2004, pp. 3227–3234.
25. Weimer, A. W., Moore, W. G., Roach, R. P., Hitt, J. E., Dixit, R. S., and Pratsinis, S. E. "Kinetics of Carbothermal Reduction Synthesis of Boron Carbide." *Journal of the American Ceramic Society*, Vol. 75, No. 9, 1992, pp. 2509–2514.
26. Jung, C. H., Lee, M. J., and Kim, C. J. "Preparation of Carbon-Free B4C Powder from B2O 3 Oxide by Carbothermal Reduction Process." *Materials Letters*, Vol. 58, No. 5, 2004, pp. 609–614.
27. Dai, J., Pineda, E. J., Bednarcyk, B. A., Singh, J., and Yamamoto, N. Macro-Scale Testing and Micromechanics Modeling of Fracture Behaviors for Boron Carbide Composites with Hierarchical Microstructures. 2021.
28. *ASTM C1421 - 18 Standard Test Methods for Determination of Fracture Toughness of Advanced Ceramics at Ambient Temperature*.
29. Aboudi, J., Pindera, M. J., and Arnold, S. M. "Linear Thermoelastic Higher-Order Theory for Periodic Multiphase Materials." *Journal of Applied Mechanics, Transactions ASME*, Vol. 68, No. 5, 2001, pp. 697–707.
30. Aboudi, J., Arnold, S., and Bednarcyk, B. *Micromechanics of Composite Materials*. Elsevier Inc., 2013.
31. ABOUDI, J. "The Generalized Method of Cells and High-Fidelity Generalized Method of Cells Micromechanical Models—A Review." *Mechanics of Advanced Materials and Structures*, Vol. 11, Nos. 4–5, 2004, pp. 329–366.
32. Bednarcyk, B. A., and Arnold, S. M. *MAC/GMC 4.0 User's Manual-Keywords Manual*. 2002.
33. Bednarcyk, B., and Arnold, S. "MAC/GMC 4. 0 User's Manual: Example Problem Manual." 2002.
34. Bažant, Z. P., and Oh, B. H. "Crack Band Theory for Fracture of Concrete." *Matériaux et Constructions*, Vol. 16, No. 3, 1983, pp. 155–177.
35. Pineda, E. J., Bednarcyk, B. A., Waas, A. M., and Arnold, S. M. *Implementation of a Smeared Crack Band Model in a Micromechanics Framework*. 2012.
36. Pineda, E. J., Bednarcyk, B. A., Waas, A. M., and Arnold, S. M. "Progressive Failure of a Unidirectional Fiber-Reinforced Composite Using the Method of Cells: Discretization Objective Computational Results." *International Journal of Solids and Structures*, Vol. 50, No. 9, 2013, pp. 1203–1216.
37. Meyer, P., and Waas, A. M. "FEM Predictions of Damage in Continous Fiber Ceramic Matrix Composites under Transverse Tension Using the Crack Band Method." *Acta Materialia*, Vol. 102, 2016, pp. 292–303.
38. White, R. M., and Dickey, E. C. "The Effects of Residual Stress Distributions on Indentation-

Induced Microcracking in B4C-TiB2 Eutectic Ceramic Composites." *Journal of the American Ceramic Society*, Vol. 94, No. 11, 2011, pp. 4032–4039.

39. White, R. M., and Dickey, E. C. "Mechanical Properties and Deformation Mechanisms of B4C-TiB2 Eutectic Composites." *Journal of the European Ceramic Society*, Vol. 34, No. 9, 2014, pp. 2043–2050.